

UniIF: Unified Molecule Inverse Folding

Zhangyang Gao[†], Jue Wang[†], Cheng Tan[†], Lirong Wu, Yufei Huang, Siyuan Li, Zhirui Ye, Stan Z. Li*
 AI Lab, Research Center for Industries of the Future, Westlake University
 {gaozhangyang, tancheng, Stan.ZQ.Li}@westlake.edu.cn

Abstract

Molecule inverse folding has been a long-standing challenge in chemistry and biology, with the potential to revolutionize drug discovery and material science. Despite specified models have been proposed for different small- or macro-molecules, few have attempted to unify the learning process, resulting in redundant efforts. Complementary to recent advancements in molecular structure prediction, such as RoseTTAFold All-Atom and AlphaFold3, we propose the unified model UniIF for the inverse folding of all molecules. We do such unification in two levels: 1) Data-Level: We propose a unified block graph data form for all molecules, including the local frame building and geometric feature initialization. 2) Model-Level: We introduce a geometric block attention network, comprising a geometric interaction, interactive attention and virtual long-term dependency modules, to capture the 3D interactions of all molecules. Through comprehensive evaluations across various tasks such as protein design, RNA design, and material design, we demonstrate that our proposed method surpasses state-of-the-art methods on all tasks. UniIF offers a versatile and effective solution for general molecule inverse folding.

1 Introduction

Molecule inverse folding plays a pivotal role in drug and material design, enabling scientists to synthesize novel molecules with the desired structure. Previously, many studies focus on either macromolecules [19, 33, 21, 9, 17, 4, 10, 17, 8, 34] or small molecules [6, 26, 16, 28, 14, 31] separately, leaving the challenge of inverse folding general molecules. For example, the advanced small molecule model [6, 31] take atoms as basic units; the macromolecule models [8, 10] consider predefined microstructures (such as amino acids and nucleotides) as the basic units. Additionally, even for the same molecule, different models employ varying strategies to extract geometric features. Complementary to the great success of RoseTTAFold All-Atom [25] and AlphaFold3 [1] in molecular structure prediction, we propose a unified model, UniIF, for the inverse folding of all molecules.

By comparing small- and macro-molecules, we identify three challenges toward the unified model: (1) **Unit Discrepancy**: The macromolecules takes predefined microstructures (amino acids and nucleotides) as the basic units, while small molecules takes atoms as basic units. (2) **Geometric Featurizer**: Different studies employ various strategies for extracting geometric features from structures, such as distance, angles and tensor product; there are lack of unified featurization strategy. (3) **System Size**: The small-molecules allow the full attention transformer to learn long-term dependencies, but the quadratic computing cost limits the mechanism scaling up to macro-molecular systems. Alternatively, previous research use sparse GNN, which suffers from the limited local receptive field that causes over-smoothing and over-squashing [29]. In addition, developing a unified model working well for all molecules is challenging.

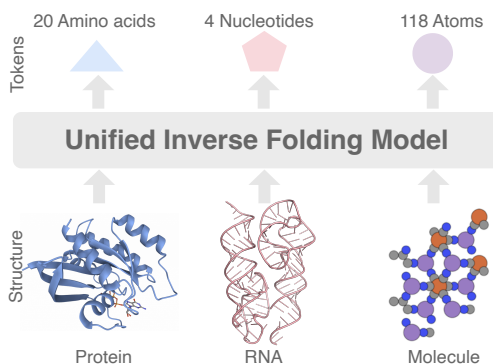


Figure 1: Unified molecule inverse folding.

[†]Equal Contribution, *Corresponding Author.

The [unit discrepancy](#) makes it challenge to adapt methods across small- and macro-molecules, which explains the divergence between these two research lines. As a solution, we propose a frame-based block to unify the representation of amino acids, nucleotides, and atoms: a group of atoms with varying size is treated as a block with fixed size. Each block includes decoupled equivariant basis and invariant features, generalizing the representation of AlphaFold2 and other small-molecule methods.

The [geometric featurizer](#) is necessary to capture the geometric interactions between blocks. We initialize the equivariant block basis using predefined rules or a learnable GNN layer, and then constructing invariant block features based on these basis. The key operation is to use local coordinates and dot product to capture the geometric interactions between virtual atoms. We reuse the featurizer in each model layer to interactively learn updated geometric features, where the concept of directed virtual atom is introduced to enhance the pairwise interactions. We show that the unified featurizer works well across protein design, RNA design, and material design.

We use sparse GNN to address the [system size](#) issue, while maintaining the ability to capture long-term dependencies. The transformer-style protein models like AlphaFold and RosettaFold require a substantial amount of GPU memory. Sparse GNNs, on the other hand, are criticized for their tendency to over-smooth and over-squash due to their limited local receptive field. To be efficient while preserving the ability to capture long-term dependencies, we introduce global virtual blocks. Each virtual block is connected to all real blocks, serving as an information exchange agent.

We conducted comprehensive experiments across various tasks, including protein design, RNA design, and material design, to demonstrate the effectiveness of UniIF. The results show that UniIF achieves state-of-the-art performance on all the tasks, which is non-trivial and may benefit the machine learning, drug discovery, and material science communities.

2 Related work

Unification. Unified molecular learning has attracted increasing attention in recent years. RoseTTAFold All-Atom (RFAA) [25] and AlphaFold3 [1] are two representative models that have achieved remarkable success in protein structure prediction. RoseTTAFold All-Atom uses an atom-bond graph for small molecules and a frame graph for macromolecules. AlphaFold3 uses a bi-level representations, i.e., atom representation and token representation, for all molecules. The token concept is equivalent to the block concept in this paper, which means a group of atoms, such as a amino acid or a nucleotide. GET [24] and EPT [20] are two recent models that use a block representation for both small and macromolecules and introduce a new equivariant transformer backbone. Unlike RFAA [25], which specifies a atom-bond graph for small molecules, our model employs a unified block graph for all molecule types and do not require the atom-bond graph. Our model also differs from AlphaFold3 [1], GET [24] and EPT [20] in the that we introduce the vector basis for each block.

Protein Inverse Folding. Recent research use k -NN graph to represent the 3D structure and employ graph neural networks for protein inverse folding. GraphTrans [19] uses the graph attention encoder and autoregressive decoder for protein design. GVP [21] proposes geometric vector perceptrons to learn from both scalar and vector features. GCA [33] introduces global graph attention for learning contextual features. In addition, ProteinSolver [32] is developed for scenarios where partial sequences are known while not reporting results on standard benchmarks. Recently, AlphaDesign [9], ProteinMPNN [4], ESMIF [17], LMDesign [40], KWDesign [8], VFN [27] achieves dramatic improvements. A benchmark [11] is proposed to comprehensively evaluate protein design models.

RNA Inverse Folding. RNA inverse folding is a challenging task due to the complex secondary structure and tertiary structure. Traditional methods [3] include colony optimization and constraint programming, in addition to adaptive walk, simulated annealing and Boltzmann sampling. Recent deep learning method RDesign [34] has achieved promising results and build a benchmark for AI researchers to follow-up. RiboDiffusion [18] use diffusion decoder to generate RNA sequences conditioned on the backbone structure embeddings.

Material Design. Deciding which chemical compositions are likely to form compounds is a critical task in material design [28, 26, 14]. An important application is to substitute lattice-site elements or ionic species within existing compounds that exhibit similar chemical behaviors. Wang et al. [36] successfully employed the elemental substitution method to discover 18,479 stable compounds out of a pool of 189,981 potential candidates. Recently, Jensen et al. [6] introduced a open dataset for material design and established a benchmark for evaluating deep learning models in this domain.

3 Method

3.1 Overall Framework

As shown in Fig. 2, we propose the unified model for general molecule inverse folding. The key insights include: (1) transforming all molecules into block graphs, where each block represents an amino acid, nucleotide, or atom; (2) proposing a geometric featurizer to initialize geometric node and edge features; and (3) introducing a new GNN layer with long-term dependencies to learn expressive block representations. Our unified model achieves competitive results across diverse tasks, including protein design, RNA design, and material design.

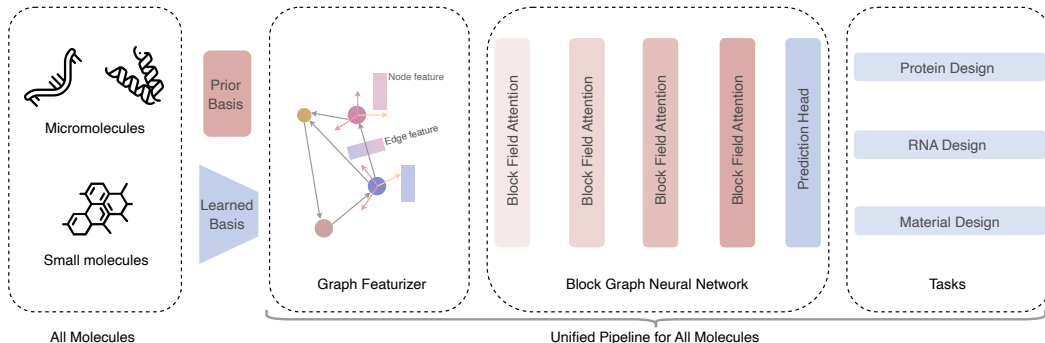


Figure 2: The Overall framework. (1) The model treat all types of molecules as block graphs. For macromolecules, we use predefined frames based on amino acids and nucleotides; for small molecules, we learn the local frame of each block by one-layer GNN. (2) A geometric featurizer is used to initialize the geometric node feature and edge features. (3) We propose the block graph attention layer, based on which we build the block graph neural network to learn expressive block representations. (4) Finally, we show that the UniIF can achieve competitive results on diverse tasks, ranging from protein design, RNA design and material design.

3.2 Block Graph

We introduce the block graph to represent all types of molecules, where the key insight is to transform irregular set of atoms (varying size) as regular block representation (fixed size).

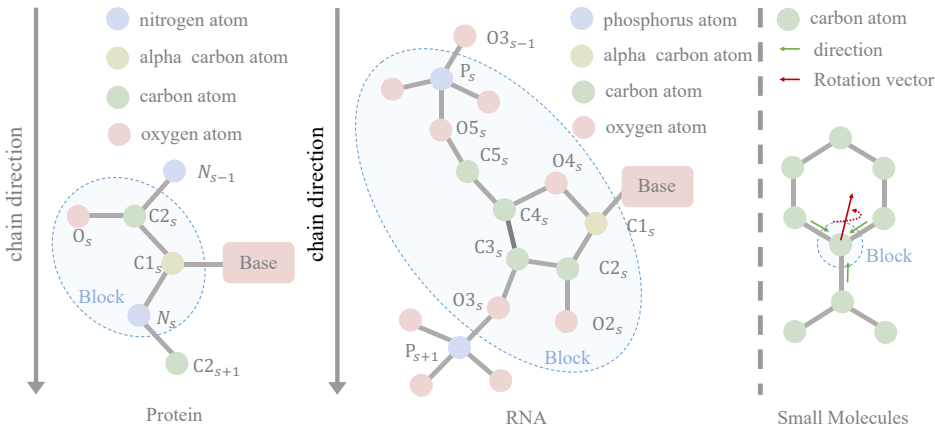


Figure 3: Blocks of different molecules. The basic building blocks include amino acids, nucleotides and atoms.

Atom-based Block Representation. A block $\mathcal{B} = \{(\mathbf{x}_i, \mathbf{z}_i)\}_{i=1}^{|\mathcal{B}|}$ contains a set of atoms $\{\mathbf{x}_i, \mathbf{z}_i\}_{i=1}^{|\mathcal{B}|}$, where $\mathbf{x}_i \in \mathbb{R}^3$ and $\mathbf{z}_i \in \mathbb{R}^d$ represent the equivariant coordinate and invariant features, such as the atom type. The common block types include amino acids, nucleotides, and atoms, which are represented as \mathcal{B}^{fold} , \mathcal{B}^{rna} , and \mathcal{B}^{smol} , respectively. Formally, we write $\mathcal{B}^{fold} = \{(\mathbf{x}_i, \mathbf{z}_i)\}_{i \in \mathcal{V}^{fold}}$ and $\mathcal{B}^{rna} = \{(\mathbf{x}_i, \mathbf{z}_i)\}_{i \in \mathcal{V}^{rna}}$, where $\mathcal{V}^{fold} = \{\text{N, C1, C2, O}\}$ and $\mathcal{V}^{rna} = \{\text{P, C5, C4, C3, C2, C1, O5, O4, O3, O2}\}$ are the sets of atoms for amino acids and nucleotides, respectively. For small molecules, each atom a represents a block $\mathcal{B}^{smol} = \{(\mathbf{x}_a, \mathbf{z}_a)\}$, where $1 \leq a \leq 118$. As the block size $|\mathcal{B}|$ varies for different types of blocks, the atom-based blocks representation could not directly be applied for unified modeling.

Frame-based Block Representation. We introduce frame-based block representation to unify the modeling of all molecules. A block $\mathcal{B} = (F, \mathbf{f})$ contains the equivariant frame F and invariant feature vector $\mathbf{f} \in \mathbb{R}^d$. The local frame $F(R, \mathbf{t})$ contains the axis matrix $R = [e_1, e_2, e_3, \dots, e_u]$ and translation vector \mathbf{t} . We set \mathbf{t} as the coordinate of the representative atom, i.e., C1 of macromolecules and the atom itself of small molecules. Following AlphaFold2, we consider the special case that $R \in \mathbb{R}^{3,3}$ is orthogonal. However, additional experiments show that the model can also work well with non-orthogonal axis matrix. For macromolecules, the axis matrix R is predefined based on amino acids and nucleotides, while for small molecules,

we learn the axis matrix R as it does not have prior common structure patterns. The frame-based block representation decouples geometric information: (1) the local frame basis describe the equivariant pose; (2) the invariant feature vector could embed the atom type and invariant local structure patterns for different tasks. More importantly, the dimension of the frame-based block representation is fixed, which is beneficial for the unified modeling; we build block features in Sec. 3.3.

Frame-based Block Graph. Given a molecule $\mathcal{M} = \{\mathcal{B}_s\}_{s=1}^n$ containing n blocks, we build the block graph $\mathcal{G}(\{\mathcal{B}_s\}_{s=1}^n, \mathcal{E})$ using kNN algorithm. In the block graph, the s -th node is represented as $\mathcal{B}_s = (F_s, \mathbf{f}_s)$, and the edge between (s, t) is represented as $\mathcal{B}_{st} = (F_{st}, \mathbf{f}_{st})$. The relative frame is defined as $F_{st} = F_s^{-1} \circ F_t$. Inspired by [22, 10, 27], we modify PiFold featurizer to initialize the geometric node feature \mathbf{f}_s and edge feature $\mathbf{f}_{s,t}$; refer to Sec. 3.3.

Relation to Other Methods. The frame-based block is a generalized data form of AlphaFold2 and other methods. If R is required to be a rotation matrix, the frame-based block is equivalent to AlphaFold2’s local frame; otherwise, it is equivalent to represent the atom as invariant feature \mathbf{h} and equivalent vector \mathbf{x} , similar to GVP [21] and DimeNet [12].

3.3 Block Graph Featurizer

Learning Local Frame. For small molecules, there is no predefined local frame, and we need to learn the local frame for each atom. Given the the molecule $\mathcal{M} = \{(\mathbf{x}_s, \mathbf{z}_s)\}_{s=1}^{|\mathcal{M}|}$, we use a 1-layer of GNN to initialize the atom representation $\{\mathbf{z}_s\}_{s=1}^{|\mathcal{M}|} \leftarrow \text{BlockGAT}(\{(\mathbf{x}_s, \mathbf{z}_s)\}_{s=1}^{|\mathcal{M}|})$, where the initial local frames are $T(\mathbf{I}, \mathbf{0})$. The rotation vector \mathbf{r}_s of the s -th atom is constructed by message passing:

$$\mathbf{r}_s = (r_x, r_y, r_z) = \sum_{k \in \mathcal{N}_s} \frac{e^{\text{MLP}(\mathbf{z}_s, \mathbf{z}_k)}}{\sum_{k \in \mathcal{N}_s} e^{\text{MLP}(\mathbf{z}_s, \mathbf{z}_k)}} \frac{\mathbf{x}_k - \mathbf{x}_s}{\|\mathbf{x}_k - \mathbf{x}_s\|} \quad (1)$$

\mathcal{N}_s is the s -th atom’s neighbor system. Let the direction $(r_x, r_y, r_z) = \frac{\mathbf{r}_s}{\|\mathbf{r}_s\|}$ and magnitude $\theta = \|\mathbf{r}_s\|$ represent the rotation axis and angle, we compute the quaternions \mathbf{q}_s and rotation matrix R_s :

$$\begin{cases} \mathbf{q}_s = [w, x, y, z] = [\cos \frac{\theta}{2}, r_x \sin \frac{\theta}{2}, r_y \sin \frac{\theta}{2}, r_z \sin \frac{\theta}{2}] \\ R_s = [e_x, e_y, e_z] = \begin{bmatrix} 1 - 2y^2 - 2z^2 & 2xy - 2zw & 2xz + 2yw \\ 2xy + 2zw & 1 - 2x^2 - 2z^2 & 2yz - 2xw \\ 2xz - 2yw & 2yz + 2xw & 1 - 2x^2 - 2y^2 \end{bmatrix} \end{cases} \quad (2)$$

Finally, the local frame of the s -th atom is $T_s(R_s, \mathbf{t}_s)$, where \mathbf{t}_s is the atom coordinate. Experiments show that learning rotation vectors consistently outperforms learning Schmidt-orthogonalized axes.

Node Geometric Feature. The invariant block feature captures the atom type and the local structure:

$$\begin{cases} \mathbf{z}_i^{\text{pos}} = R_s^T(\mathbf{x}_i - \mathbf{t}_s) = F_s^{-1} \circ \mathbf{x}_i & \text{Equivalent to invariant features, local structure} \\ \mathbf{f}_s = \frac{1}{|\mathcal{B}_s|} \sum_{i \in \mathcal{B}_s} \text{MLP}(\mathbf{z}_i, \mathbf{z}_i^{\text{pos}}) & \text{Pooling atom features as block features, embed atom type} \end{cases} \quad (3)$$

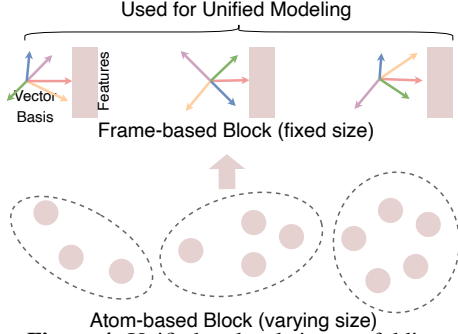


Figure 4: Unified molecule inverse folding.

The inverse frame operation T_s^{-1} project the equivalent global coordinates to the invariant local coordinate, i.e., $\mathbf{x}^{local} = F_s^{-1} \circ \mathbf{x}^{global} = R_s^T(\mathbf{x}^{global} - \mathbf{t}_s)$. We use MLP to embed atom type and local coordinates. All atom features in the same block are pooled to get the block feature \mathbf{f}_s .

Edge Geometric Feature. We initialize pairwise features following the principle that

Edge features capture the directed 3D interactions.

Instead of using mutually constructed distance and angle features, we concatenate the local coordinates of two blocks to fully describe their 3D positions. Given \mathcal{B}_s and \mathcal{B}_t with global coordinate matrices as $X_s \in \mathbb{R}^{|v_s|,3}$ and $X_t \in \mathbb{R}^{|v_t|,3}$, the invariant edge features following $s \leftarrow t$ direction is

$$\mathbf{f}_{s,t} = T_s^{-1} \circ ([X_s \| X_t]) \quad (4)$$

where $T_s^{-1} = (R_s^T, -R_s^T \mathbf{t}_s)$ projects equivariant global coordinates to invariant local coordinates.

3.4 Block Graph Attention Module

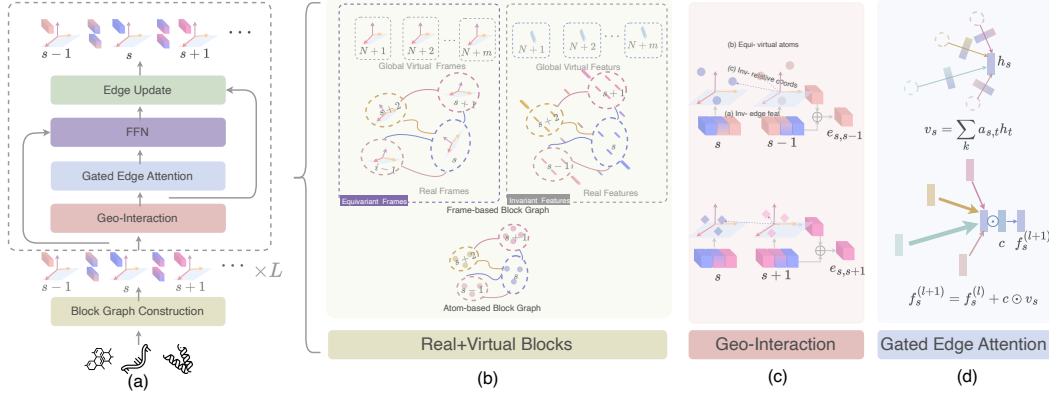


Figure 5: Block Graph Attention Module. (a) Virtual Block for Long-term Dependencies. (b) Geometric Interaction Extractor for learning pairwise features. (c) Gated Edge Attention for updating node features.

Frame-based SE-(3) Module Design. Given the geometric transformation $\mathbf{y} = W\mathbf{x}$, we decompose $W = R_t \Sigma R_s^T$ using SVD and explain $\mathbf{y} = R_t \Sigma R_s^T \mathbf{x}$ as:

1. Projecting \mathbf{x} as the local coordinate \mathbf{x}^{local} using the frame $F_s(R_s, \mathbf{0})$, i.e., $\mathbf{x}^{local} = R_s^T \mathbf{x}$.
2. Updating local coordinates via gated attention, i.e., $\mathbf{x}^{local} \leftarrow \Sigma \mathbf{x}^{local}$.
3. Translating \mathbf{x}^{local} as the global coordinate using frame $T_t(R_t, \mathbf{0})$, i.e., $\mathbf{y} = R_t \mathbf{x}^{local}$.

If we parameterize $\Sigma \mathbf{y}$ as $f_\theta(\mathbf{y})$, and considers the effects of translation, i.e., $T_s(R_s, \mathbf{t}_s), T_t(R_t, \mathbf{t}_t)$, the general principle of designing SE-(3) networks could be:

$$\begin{cases} \hat{\mathbf{z}} = R_s^{-1}(\mathbf{x} - \mathbf{t}_s) = T_s^{-1} \circ \mathbf{x} & \text{Equivalent to invariant} \\ \hat{\mathbf{z}} \leftarrow f_\theta(\hat{\mathbf{z}}) & \text{Invariant update, one can use GNN or Transformer} \\ \hat{\mathbf{x}} = R_t \hat{\mathbf{y}} + \mathbf{t}_t = T_t \circ \hat{\mathbf{z}} & \text{Invariant to equivalent} \end{cases} \quad (5)$$

The well-known AlphaFold actually follows such a design, where they parameterize f_θ as the IPA module. In this work, we replace f_θ with an enhanced graph neural network:

$$\mathbf{f}_s^{(l+1)}, \mathbf{f}_{st}^{(l+1)} \leftarrow f_\theta(\mathbf{f}_s^{(l)}, \mathbf{f}_{st}^{(l)} | T_s, T_{st}, \mathcal{E}) \quad (6)$$

where $\mathbf{f}_s^{(l)}$ and $\mathbf{f}_{st}^{(l)}$ represent the input node and edge features of the l -th layer. In Fig. 5, we show the design of the Block Graph Attention Module, consisting of three components: (1) geometric interaction extractor, (2) virtual block for long-term dependencies, and (3) the edge attention mechanism. We show the detailed design of the Block Graph Attention Module in the following sections.

Long-term Dependency via Virtual Blocks. The GNN is criticized by local receptive field, yielding the problem of over-smoothing and over-squashing [2, 5, 29, 13]. Transformers overcome these problems using direct paths between distant nodes, while suffering from the $\mathcal{O}(n^2)$ computing cost. We introduce n' virtual blocks $\{\mathcal{B}_i\}_{i=n}^{n+n'}$ as information agents for a graph. Each virtual block directly connects to all the real blocks, resulting in $(2 \cdot n \cdot n')$ additional directed edges. As $n' \ll n$, we claim that the computing cost is close to original GNN. All the virtual blocks, i.e., $T_{n+1}(R', \mathbf{t}'), T_{n+2}(R', \mathbf{t}'), \dots, T_{n+n'}(R', \mathbf{t}')$, share the same rotation R' and translation \mathbf{t}' :

$$\begin{cases} \mathbf{X} = [\mathbf{x}_1, \mathbf{x}_2, \dots] & \text{All the coordinates of the molecule} \\ \mathbf{X}^T \mathbf{X} = U \Lambda V^T & \text{SVD} \\ R' = UV^T = [e_x, e_y, e_z] \\ \mathbf{t}' = \frac{\sum_{i=1}^N \mathbf{x}_i}{N} & \text{Center of Mass} \end{cases} \quad (7)$$

The invariant features of virtual blocks are different, as we hope they learn diverse interactions. We encode the index to initialize block features $\mathbf{f}'_i = \text{Embedding}(i)$ for $i \in \{1, 2, \dots, n'\}$.

Geometric Interaction Extractor. We enhance edge features with geometric interactions using the local coordinates of virtual inter-atoms and dot products of virtual intra-atoms. Previous works, such as PiFold [10], introduced virtual atoms in the featurizer to capture informative side-chain geometry beyond protein backbones, resulting in performance gains. VFN [27] extended this idea by allowing GNN layers to update the virtual atoms. However, these efforts are limited to learning virtual intra-atoms conditioned on node features. Instead, we propose virtual inter-atoms conditioned on edge features, allowing the same node to exhibit different virtual states specified by edges. Additionally, inspired by small molecule modeling, we use the dot product of virtual intra-atoms to capture angle information. We show the geometric interactions in Fig. 6, and formulate it as:

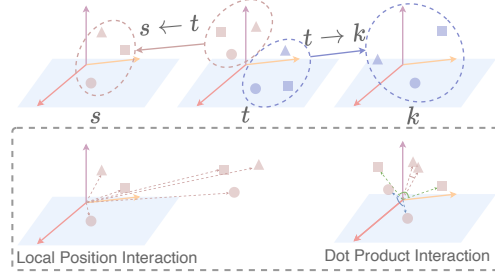


Figure 6: Geometric Interactions.

Additionally, inspired by small molecule modeling, we use the dot product of virtual intra-atoms to capture angle information. We show the geometric interactions in Fig. 6, and formulate it as:

$$\begin{cases} \mathbf{h}_{st}^{(l)}, \mathbf{h}_t^{(l)} = \text{MLP}(\mathbf{f}_{st}^{(l)}), \text{MLP}(\mathbf{f}_t^{(l)}) \in \mathbb{R}^{m,3} & \text{Edge feature} \\ \hat{\mathbf{z}}_{st}^{(l)} = (T_{st} \circ \mathbf{h}_{st}^{(l)}) \parallel \mathbf{h}_{st}^{(l)} & \text{Local coordinates of virtual inter-atoms} \\ \mathbf{a}_{st} = \mathbf{h}_s^T R_s^T R_t \mathbf{h}_t & \text{Geometric dot product of virtual intra-atoms} \\ \mathbf{g}_{st}^{(l)} = \text{MLP}(\hat{\mathbf{z}}_{st}^{(l)}, q_{st}, r_{st}, \mathbf{a}_{st}) \\ \mathbf{f}_{st}^{(l)} \leftarrow \text{MLP}(\mathbf{f}_{st}^{(l)}, \mathbf{g}_{st}^{(l)}) \end{cases} \quad (8)$$

where $T_{st} = T_s^{-1} \circ T_t = (R_s^{-1} R_t, R_s^{-1}(\mathbf{t}_t - \mathbf{t}_s))$, $q_{st} = \text{vec}(R_{st}) \in \mathbb{R}^9$ is the flatten rotation matrix of T_{st} , and $r_{st} = \|\mathbf{t}_s - \mathbf{t}_t\|$ indicates the pairwise distance. All q_{st} , r_{st} and \mathbf{a}_{st} are invariant features. We highlight the difference to previous researches in color.

Gated Edge Attention. We modify PiFold’s GNN to capture the geometric interactions when updating node features. For molecular design tasks, we find that aggregating edge features only leads to consistent performance gains. We understand this phenomenon as the model can pay more attention on learning 3D interactions under such a model design. In addition, we use a gated mechanism to control how the edge features are injected to node features. The gated edge attention module is:

$$\begin{cases} w_{st} = \text{AttMLP}(\mathbf{f}_s^{(l)} \parallel \mathbf{f}_{st}^{(l)} \parallel \mathbf{f}_t^{(l)}) \\ a_{st} = \frac{\exp w_{st}}{\sum_{k \in \mathcal{N}_s} \exp w_{sk}} \\ \mathbf{h}_t^{(l)} = \text{EdgeMLP}(\mathbf{f}_{st}^{(l)}) & \text{Only condition on edge} \\ \Delta \mathbf{f}_s^{(l)} = \sum_{t \in \mathcal{N}_s} a_{st} \mathbf{h}_t^{(l)} \\ \mathbf{f}_s^{(l+1)} = \mathbf{f}_s^{(l)} + \sigma(\text{MLP}(\Delta \mathbf{f}_s^{(l)})) \odot \Delta \mathbf{f}_s^{(l)} & \text{Update node feature via forget gate} \end{cases} \quad (9)$$

where \odot is element-wise product operation, and $\sigma(\cdot)$ is the sigmoid function. We highlight the difference between PiGNN and the proposed module in color.

FFN & Edge Updating. Analogous to the transformer model, the FFN is a MLP. The edge updating layer remains the same as PiFold:

$$\mathbf{f}_{st} = \text{EdgeMLP}(\mathbf{f}_s || \mathbf{f}_{st} || \mathbf{f}_t) \quad (10)$$

The proposed module could be equivalently implemented as a transformer module using matrix multiplication. However, we find that padding proteins to the maximum length would greatly increase the computing cost in both GPU occupancy and runtime; We suggest using GNN without padding.

Regularization. We find that the proposed model fit training data better than PiFold and more likely to suffer from overfitting. To address this issue, we randomly drop out the nodes/edges with a probability of p to prevent overfitting. We find that controlling the dropout rate could result in models with different fitting abilities. The best performance is achieved when $p = 0.05$.

4 Experiments

We show the effectiveness of UniIF via multiple inverse folding tasks and ablation studies. We briefly introduce molecular design tasks as follows:

- **Protein Design (T1):** Designing protein sequences folding into the target structure.
- **RNA Design (T2):** Designing RNA sequences folding into the target structure.
- **Material Design (T3):** Discovering stable composition from a known material structure.

4.1 Protein Design (T1)

Task Description Protein design aims to design protein sequences that fold into target structures. Given a protein backbone structure $\mathcal{X} = \{X_i \in \mathbb{R}^{m,3} : 1 \leq i \leq n\}$, where m is the maximum number of points belonging to the i -th residue, n is the number of residues and the natural proteins are composed by 20 types of amino acids, the goal is to learn a function \mathcal{F}_θ :

$$\mathcal{F}_\theta : \mathcal{X} \mapsto \hat{\mathcal{S}}. \quad (11)$$

The parameters θ are learned by minimizing the cross-entropy loss, i.e., $\mathcal{L}(\mathcal{F}_\theta(\mathcal{X}), \mathcal{S}) = -\sum_{i=1}^n \log s_i p(\hat{s}_i | \mathcal{X}, \theta)$. The task is challenging due to the combinatorial search space of amino acids and the complex relationship between sequence and structure.

Settings We evaluate of UniIF on the CATH4.3 dataset [30] following prior works [11, 8]. The dataset is split by the CATH topology classification code, yielding 16,631 training, 1,516 validation, and 1,864 testing samples. To assess generalization, we adopt a time-split strategy, considering the use of pretrained ESM2 models by some baselines, which risk data leakage. The time-split evaluation assigns data before a specific date to the training set and data after that date to the test set. For structural time-split evaluation, we use the CASP15 dataset [11], containing novel crystal structures not seen during training. For sequence time-split evaluation, we use the NovelPro dataset [8], which includes 76 protein sequences released within 30 days before November 23, 2023, with structures predicted by AlphaFold2. UniIF consists of 10 layers of BlockGAT with a hidden dimension of 128. It is trained using the Adam optimizer with a learning rate of 1e-3 and a batch size of 8 for 50 epochs.

Metrics & Baselines We report the median recovery rate of the top-1 predicted sequences, representing the percentage of correctly predicted residues. The ESM2-free baselines include StructGNN [19], GraphTrans [19], GCA [33], GVP [21], AlphaDesign [9], ProteinMPNN [4], and PiFold [10]. The ESM2-based baselines include LMDesign [17] and KWDesign [8]. While we prefer open-source baselines, we also re-implement VFN [27] for a comprehensive comparison.

Conclusion We provide results under different settings (with and without ESM2) and across diverse datasets (CATH4.3, CASP, NovelPro). Using a pure inverse folding model without ESM2, UniIF achieves the best performance on all datasets, demonstrating its effectiveness. Notably, UniIF outperforms the strong baseline PiFold with fewer learnable parameters. In time-split evaluations, UniIF surpasses all baselines, including ESM2-based methods, by a significant margin. On NovelPro, which features novel sequences, UniIF outperforms LMDesign and KWDesign that use ESM2 for sequence refinement. This indicates UniIF’s superior generalizability, crucial for real-world

w ESM	Model length	Rec % \uparrow (CATH4.3)				Full	Rec % \uparrow CASP	Rec % \uparrow NovelPro	Params
		$L < 100$	$100 \leq L < 300$	$300 \leq L < 500$					
✓	LMDesign [17]	0.47	0.56	0.61	0.56	0.48	0.59		
	KWDesign [8]	0.51	0.61	0.69	0.60	0.56	0.64		
✗	StructGNN [19]	0.30	0.34	0.40	0.34	0.36	0.40	1.4M	
	GraphTrans [19]	0.29	0.34	0.39	0.34	0.35	0.40	1.5M	
	GCA [33]	0.32	0.36	0.41	0.36	0.40	0.43	2.1M	
	GVP [21]	0.33	0.38	0.45	0.38	0.39	0.42	0.9M	
	AlphaDesign [9]	0.37	0.43	0.47	0.42	0.42	0.46	3.6M	
	ProteinMPNN [4]	0.38	0.44	0.52	0.44	0.44	0.52	1.7M	
	PiFold [10]	0.43	0.52	0.59	0.51	0.47	0.57	5.8M	
	UniIF (ours)	0.45	0.54	0.61	0.53	0.51	0.66	5.4M	
Ablation	VFN [27]	0.45	0.53	0.60	0.52	0.48	0.63	5.4M	
	-GDP	0.45	0.53	0.61	0.52	0.50	0.65	5.3M	
	-EAttn	0.44	0.53	0.60	0.52	0.48	0.63	5.7M	
	-VFrame	0.45	0.53	0.61	0.52	0.49	0.64	5.4M	

Table 1: Protein Design results. The **best** and suboptimal results are labeled with bold and underlined. "VFN" means that we replace the geometric interaction operation with VFN's operation [27]. "-GDP" means that we remove the geometric dot product features. "-EAttn" means that we replace the gated edge attention with PiGNN's attention module [10]. "-VFrame" means that we remove the global virtual frames.

applications. Ablation studies show that the proposed geometric featurizer, gated edge attention, and global virtual frame enhance performance. On CATH4.3, the overall improvement is slight due to strong baselines, but time-split evaluation highlights UniIF's superiority in generalization.

4.2 RNA Design (T2)

Task Description Similar to protein design, RNA design aims to design RNA sequences that fold into target structures. Specially, previous work [34] use the RNA secondary structure as additional input to guide the design process, since the tertiary structure is limited. In this work, we only use the tertiary structures as input for the reason of unification, which is more challenging than the baselines.

Datasets & Baselines We conduct experiments RNA on the dataset collected by RDesign [34], consisting of 2218 RNA tertiary structures, which are divided into training (1774 structures), testing (223 structures), and validation (221 structures) sets based on their structural similarity. Following RDesign's benchmark, baseline methods include SeqRNN, SeqLSTM, StructMLP, StructGNN, and StructGNN, GraphTrans [19], PiFold [10] and RDesign [34]. Given the small number of data samples, we report the median recovery and its standard deviation for three independent runs.

Table 2: The recovery of RNA design. The **best** and suboptimal results are labeled with bold and underlined.

Method	Recovery (%) \uparrow			
	Short	Medium	Long	All
SeqRNN (h=128)	26.52 \pm 1.07	24.86 \pm 0.82	27.31 \pm 0.41	26.23 \pm 0.87
SeqRNN (h=256)	27.61 \pm 1.85	27.16 \pm 0.63	28.71 \pm 0.14	28.24 \pm 0.46
SeqLSTM (h=128)	23.48 \pm 1.07	26.32 \pm 0.05	26.78 \pm 1.12	24.70 \pm 0.64
SeqLSTM (h=256)	25.00 \pm 0.00	26.89 \pm 0.35	28.55 \pm 0.13	26.93 \pm 0.93
StructMLP	25.72 \pm 0.51	25.03 \pm 1.39	25.38 \pm 1.89	25.35 \pm 0.25
StructGNN	27.55 \pm 0.94	28.78 \pm 0.87	28.23 \pm 1.95	28.23 \pm 0.71
GraphTrans [19]	26.15 \pm 0.93	23.78 \pm 1.11	23.80 \pm 1.69	24.73 \pm 0.93
PiFold [10]	24.81 \pm 2.01	25.90 \pm 1.56	23.55 \pm 4.13	24.48 \pm 1.13
RDesign [34]	37.22 \pm 1.14	44.89 \pm 1.67	43.06 \pm 0.08	41.53 \pm 0.38
UniIF (drop 0.05)	48.21 \pm 0.95	49.66 \pm 1.28	37.29 \pm 0.17	48.94 \pm 0.37
UniIF (drop 0.0)	42.86 \pm 0.87	48.45 \pm 1.04	39.23 \pm 0.09	44.29 \pm 0.29
UniIF (drop 0.1)	45.21 \pm 0.98	51.70 \pm 1.26	40.30 \pm 0.14	46.00 \pm 0.38
UniIF (drop 0.2)	46.97 \pm 1.04	48.11 \pm 1.37	42.00 \pm 0.18	47.19 \pm 0.45

Conclusion As shown in Table 2, UniIF achieves the best performance in all cases. The improvement is significant, as previous strong baselines like PiFold only excelled in protein design. To our knowledge, UniIF is the first model to achieve state-of-the-art performance in both protein and RNA design tasks, demonstrating its versatility and effectiveness. Compared to RDesign, which uses additional secondary structure features, UniIF relies solely on tertiary structure input and still performs better. UniIF successfully unifies the protein and RNA design processes, paving the way for a unified inverse folding model for protein-RNA complexes in future developments.

4.3 Material Design (T3)

Task Description Discovering stable atom compositions from known material structures is crucial for new material discovery [28, 26, 14]. This task is challenging due to the large composition space and the lack of large-scale data. Thanks to recent benchmark efforts [6], we can evaluate the performance of UniIF on this novel task.

Datasets & Baselines We evaluated UniIF on the CHILI-3K dataset [6], which consists of nanomaterial graphs derived from mono-metal oxides. The dataset includes 53 metallic elements and one non-metallic element (oxygen), comprising 3,180 graphs, 6,959,085 nodes, and 49,624,440 edges. Following the official benchmark, the dataset is randomly split into training (80%), validation (10%), and testing (10%) sets. Baselines include GCN [23], PMLP [39], GraphSAGE [15], GAT [35], GraphUNet [7], GIN [38], and EdgeCNN [37]. Experiments are repeated three times with different seeds, using early stopping with a patience of 50 epochs, and trained up to 1000 epochs.

Method	Rec % \uparrow
Random	1.6 \pm 0.0
GCN [23]	49.6 \pm 0.1
PMLP [39]	46.1 \pm 0.0
GraphSAGE [15]	49.1 \pm 0.4
GAT [35]	46.1 \pm 0.0
GraphUNet [7]	55.2 \pm 7.9
GIN [38]	58.7 \pm 0.2
EdgeCNN [37]	63.2 \pm 0.9
UniIF (ours)	75.3\pm1.2
- frame	54.9 \pm 2.8
- quat	65.2 \pm 3.9

Conclusion In Table 3, UniIF outperforms all baselines by a large margin. Ablation studies demonstrate the crucial role of the learned local frame in enhancing interaction feature extraction. In addition, how to learn the local frame is also important. In the "- quat" ablation, we try to learn the x, y, and z axes with Householder orthogonalization directly, but found it less effective, with the recovery rate dropping from 75.3% to 65.2%. This highlights the value of the proposed local frame learning mechanism.

Table 3: CHILI-3K Results.

4.4 Case Study

In Fig. 7, we show the designed protein and RNA sequences. In addition, we use AlphaFold3 [1] to re-fold the designed sequences into structures. The ground truth (gray), PiFold (green), and UniIF (pink) structures are aligned and compared. We observe that UniIF improves both the recovery and RMSD of the designed protein and RNA, demonstrating its effectiveness in inverse folding tasks.



Figure 7: Designed examples. The ground truth (gray), PiFold (green), and UniIF (pink) structures are aligned.

5 Conclusion

We propose the first unified model, dubbed UniIF, for general molecule inverse folding. The key points include unifying the data representation, the featurizer and the model architecture without a drop in performance. Extensive experiments show that UniIF surpasses baseline methods on all tasks. Ablation studies reveal that the geometric interaction extractor, gated edge attention, and virtual long-term dependency modules contribute to performance gains. We believe that the proposed model can benefit multiple domains, such as machine learning, drug design, and material design.

References

- [1] Josh Abramson, Jonas Adler, Jack Dunger, Richard Evans, Tim Green, Alexander Pritzel, Olaf Ronneberger, Lindsay Willmore, Andrew J Ballard, Joshua Babrick, et al. Accurate structure prediction of biomolecular interactions with alphafold 3. *Nature*, pages 1–3, 2024.
- [2] Uri Alon and Eran Yahav. On the bottleneck of graph neural networks and its practical implications. In *International Conference on Learning Representations*, 2020.
- [3] Alexander Churkin, Matan Drory Retwitzer, Vladimir Reinharz, Yann Ponty, Jérôme Waldispühl, and Danny Barash. Design of rnas: comparing programs for inverse rna folding. *Briefings in bioinformatics*, 19(2):350–358, 2018.
- [4] Justas Dauparas, Ivan Anishchenko, Nathaniel Bennett, Hua Bai, Robert J Ragotte, Lukas F Milles, Basile IM Wicky, Alexis Courbet, Rob J de Haas, Neville Bethel, et al. Robust deep learning based protein sequence design using proteinmpnn. *bioRxiv*, 2022.
- [5] Francesco Di Giovanni, Lorenzo Giusti, Federico Barbero, Giulia Luise, Pietro Lio, and Michael M Bronstein. On over-squashing in message passing neural networks: The impact of width, depth, and topology. In *International Conference on Machine Learning*, pages 7865–7885. PMLR, 2023.
- [6] Ulrik Friis-Jensen, Frederik L Johansen, Andy S Anker, Erik B Dam, Kirsten MØ Jensen, and Raghavendra Selvan. Chili: Chemically-informed large-scale inorganic nanomaterials dataset for advancing graph machine learning. *arXiv preprint arXiv:2402.13221*, 2024.
- [7] Hongyang Gao and Shuiwang Ji. Graph u-nets. In *international conference on machine learning*, pages 2083–2092. PMLR, 2019.
- [8] Zhangyang Gao, Cheng Tan, Xingran Chen, Yijie Zhang, Jun Xia, Siyuan Li, and Stan Z Li. Kw-design: Pushing the limit of protein design via knowledge refinement. In *The Twelfth International Conference on Learning Representations*, 2023.
- [9] Zhangyang Gao, Cheng Tan, Stan Li, et al. Alphadesign: A graph protein design method and benchmark on alphafolddb. *arXiv preprint arXiv:2202.01079*, 2022.
- [10] Zhangyang Gao, Cheng Tan, and Stan Z. Li. Pifold: Toward effective and efficient protein inverse folding. In *International Conference on Learning Representations*, 2023.
- [11] Zhangyang Gao, Cheng Tan, Yijie Zhang, Xingran Chen, Lirong Wu, and Stan Z Li. Proteininvbench: Benchmarking protein inverse folding on diverse tasks, models, and metrics. *Advances in Neural Information Processing Systems*, 36, 2024.
- [12] Johannes Gasteiger, Janek Groß, and Stephan Günnemann. Directional message passing for molecular graphs. *arXiv preprint arXiv:2003.03123*, 2020.
- [13] Jhony H Giraldo, Konstantinos Skianis, Thierry Bouwmans, and Fragkiskos D Malliaros. On the trade-off between over-smoothing and over-squashing in deep graph neural networks. In *Proceedings of the 32nd ACM International Conference on Information and Knowledge Management*, pages 566–576, 2023.
- [14] Sean D Griesemer, Yi Xia, and Chris Wolverton. Accelerating the prediction of stable materials with machine learning. *Nature Computational Science*, 3(11):934–945, 2023.
- [15] Will Hamilton, Zhitao Ying, and Jure Leskovec. Inductive representation learning on large graphs. *Advances in neural information processing systems*, 30, 2017.
- [16] Geoffroy Hautier, Christopher C Fischer, Anubhav Jain, Tim Mueller, and Gerbrand Ceder. Finding nature’s missing ternary oxide compounds using machine learning and density functional theory. *Chemistry of Materials*, 22(12):3762–3767, 2010.
- [17] Chloe Hsu, Robert Verkuil, Jason Liu, Zeming Lin, Brian Hie, Tom Sercu, Adam Lerer, and Alexander Rives. Learning inverse folding from millions of predicted structures. *bioRxiv*, 2022.
- [18] Han Huang, Ziqian Lin, Dongchen He, Liang Hong, and Yu Li. Ribodiffusion: Tertiary structure-based rna inverse folding with generative diffusion models. *bioRxiv*, pages 2024–04, 2024.
- [19] John Ingraham, Vikas Garg, Regina Barzilay, and Tommi Jaakkola. Generative models for graph-based protein design. *Advances in neural information processing systems*, 32, 2019.

- [20] Rui Jiao, Xiangzhe Kong, Ziyang Yu, Wenbing Huang, and Yang Liu. Equivariant pretrained transformer for unified geometric learning on multi-domain 3d molecules. [arXiv preprint arXiv:2402.12714](#), 2024.
- [21] Bowen Jing, Stephan Eismann, Patricia Suriana, Raphael JL Townshend, and Ron Dror. Learning from protein structure with geometric vector perceptrons. [arXiv preprint arXiv:2009.01411](#), 2020.
- [22] John Jumper, Richard Evans, Alexander Pritzel, Tim Green, Michael Figurnov, Olaf Ronneberger, Kathryn Tunyasuvunakool, Russ Bates, Augustin Žídek, Anna Potapenko, et al. Highly accurate protein structure prediction with alphafold. *Nature*, 596(7873):583–589, 2021.
- [23] Thomas N Kipf and Max Welling. Semi-supervised classification with graph convolutional networks. [arXiv preprint arXiv:1609.02907](#), 2016.
- [24] Xiangzhe Kong, Wenbing Huang, and Yang Liu. Generalist equivariant transformer towards 3d molecular interaction learning. [arXiv preprint arXiv:2306.01474](#), 2023.
- [25] Rohith Krishna, Jue Wang, Woody Ahern, Pascal Sturmfels, Preetham Venkatesh, Indrek Kalvet, Gyu Rie Lee, Felix S Morey-Burrows, Ivan Anishchenko, Ian R Humphreys, et al. Generalized biomolecular modeling and design with rosettafold all-atom. *Science*, 384(6693):ead12528, 2024.
- [26] Yue Liu, Tianlu Zhao, Wangwei Ju, and Siqi Shi. Materials discovery and design using machine learning. *Journal of Materiomics*, 3(3):159–177, 2017.
- [27] Weian Mao, Muzhi Zhu, Zheng Sun, Shuaike Shen, Lin Yuanbo Wu, Hao Chen, and Chunhua Shen. De novo protein design using geometric vector field networks. [arXiv preprint arXiv:2310.11802](#), 2023.
- [28] Bryce Meredig, Ankit Agrawal, Scott Kirklin, James E Saal, Jeff W Doak, Alan Thompson, Kunpeng Zhang, Alok Choudhary, and Christopher Wolverton. Combinatorial screening for new materials in unconstrained composition space with machine learning. *Physical Review B*, 89(9):094104, 2014.
- [29] Khang Nguyen, Nong Minh Hieu, Vinh Duc Nguyen, Nhat Ho, Stanley Osher, and Tan Minh Nguyen. Revisiting over-smoothing and over-squashing using ollivier-ricci curvature. In *International Conference on Machine Learning*, pages 25956–25979. PMLR, 2023.
- [30] Christine A Orengo, Alex D Michie, Susan Jones, David T Jones, Mark B Swindells, and Janet M Thornton. Cath—a hierarchic classification of protein domain structures. *Structure*, 5(8):1093–1109, 1997.
- [31] Rafael Sarmiento-Perez, Tiago FT Cerqueira, Sabine Korbel, Silvana Botti, and Miguel AL Marques. Prediction of stable nitride perovskites. *Chemistry of Materials*, 27(17):5957–5963, 2015.
- [32] Alexey Strokach, David Becerra, Carles Corbi-Verge, Albert Perez-Riba, and Philip M Kim. Fast and flexible protein design using deep graph neural networks. *Cell Systems*, 11(4):402–411, 2020.
- [33] Cheng Tan, Zhangyang Gao, Jun Xia, and Stan Z Li. Generative de novo protein design with global context. [arXiv preprint arXiv:2204.10673](#), 2022.
- [34] Cheng Tan, Yijie Zhang, Zhangyang Gao, Bozhen Hu, Siyuan Li, Zicheng Liu, and Stan Z Li. Hierarchical data-efficient representation learning for tertiary structure-based rna design. In *The Twelfth International Conference on Learning Representations*, 2023.
- [35] Petar Velickovic, Guillem Cucurull, Arantxa Casanova, Adriana Romero, Pietro Lio, Yoshua Bengio, et al. Graph attention networks. *stat*, 1050(20):10–48550, 2017.
- [36] Hai-Chen Wang, Silvana Botti, and Miguel AL Marques. Predicting stable crystalline compounds using chemical similarity. *npj Computational Materials*, 7(1):12, 2021.
- [37] Yue Wang, Yongbin Sun, Ziwei Liu, Sanjay E Sarma, Michael M Bronstein, and Justin M Solomon. Dynamic graph cnn for learning on point clouds. *ACM Transactions on Graphics (tog)*, 38(5):1–12, 2019.
- [38] Keyulu Xu, Weihua Hu, Jure Leskovec, and Stefanie Jegelka. How powerful are graph neural networks? [arXiv preprint arXiv:1810.00826](#), 2018.

- [39] Chenxiao Yang, Qitian Wu, Jiahua Wang, and Junchi Yan. Graph neural networks are inherently good generalizers: Insights by bridging gnns and mlps. [arXiv preprint arXiv:2212.09034](#), 2022.
- [40] Zaixiang Zheng, Yifan Deng, Dongyu Xue, Yi Zhou, Fei Ye, and Quanquan Gu. Structure-informed language models are protein designers. [bioRxiv](#), pages 2023–02, 2023.